Journal of Applied Research in Technology & Engineering

7(2): e25796, 2026
https://doi.org/10.4995/jarte.2026.25796

Received: January 27, 2026; Accepted: March 01, 2026;
Available online: July 13 2026; Published: July 31, 2026
ISSN 2695-8821

STUDY OF THE EFFECTS OF WINDSHIELD ANGLE ON THE DRAG FORCE OF CARS

Boyuan Du, Peng Hu*, Wenyao Zoa, Xiangyu Xin

[a] CRRC Technology Innovation (Beijing) Co., Ltd, Beijing, 100095, China.

[a1] dbyuan19981201@gmail.com, [a2] hupeng.kc@crrcgc.cc, [a3] ximeng.kcgs@crrcgc.cc, [a4] 016900010018@crrcgc.cc

Highlights:

- A nearly linear relationship between windshield angle and Cd is revealed, with values rising from 0.346 to 0.415.
- Mesh independence, y+ validation, and Cd stabilization criteria ensure the reliability of the parametric trends observed.
- Pressure and velocity analyses show steeper windshields amplify stagnation and enlarge low-velocity zones at the base.
- The drag increase is driven primarily by higher pressure drag on the windshield rather than by wake modifications.
- The numerical setup agrees with the official Cd value within 2.1%, confirming the reliability of the simplified model.

Abstract:

Vehicle aerodynamic drag significantly affects fuel efficiency at highway speeds. The windshield angle influences drag, but its quantitative effect on sport utility vehicles (SUVs) remains underexplored. This study investigates the relationship between windshield inclination and drag coefficient using computational fluid dynamics. To this end, a simplified 3D model of a 2013 BMW X5 was constructed in SolidWorks. Steady-state CFD simulations were performed in ANSYS Fluent using the pressure-based solver and RNG k-ε turbulence model with standard wall functions. The windshield angle varied from 30° to 90° in 5° increments. A mesh independence study, near-wall y+ verification, and explicit convergence criteria based on drag stabilization were implemented to ensure methodological robustness. The results show that the drag coefficient increases nearly linearly with windshield angle, from 0.346 at 30° to 0.415 at 90°. Pressure contour analysis shows surface pressure on the windshield rises from 14.2 Pa at 30° to 26.3 Pa at 90°. Velocity fields reveal enlarged low-velocity zones at the windshield base as angle steepens. Overall, the increased drag is predominantly attributable to higher pressure drag on forward-facing surfaces rather than to substantial modifications in the base wake structure. The results offer quantitative guidance for optimizing windshield design to balance aerodynamics and ergonomics in SUVs.

Keywords: windshield angle; automotive aerodynamics; computational fluid dynamics (CFD); drag coefficient (Cd); vehicle aerodynamic optimization.

Cite as: Du, B., Hu, P., Zou, W., & Xin, X. (2026). Study of the effects of windshield angle on the drag force of cars. *Journal of Applied Research in Technology & Engineering, 7*(2), e25796. https://doi.org/10.4995/jarte.2026.25796

1. Introduction

The automotive industry has studied efficiency enhancements for several decades, as fuel economy is a significant challenge confronting internal combustion engines. Due to the high demand for fossil fuels, the primary concern of designers has been maximizing engine efficiency by minimizing energy losses, while increasing the car's aerodynamics was a secondary factor in enhancing fuel efficiency (Heald, 1933). Currently, the development of technologies to improve engine efficiency is nearly at its limit, and thus, research is focusing on enhancing the performance of vehicles by improving their aerodynamics.

The challenge of automotive design lies in striking a compromise between ergonomic requirements—such as driver visibility and passenger headroom—and aerodynamic efficiency, as the vehicle shape must simultaneously satisfy both sets of constraints. Besides, the resistance encountered by the vehicle when running on a level road includes aerodynamic drag and rolling resistance, which have a specific impact when the car is running at high speed. Relevant studies have shown that when the vehicle speed reaches 80 km/h, both these resistant types are basically equal. Accordingly, when the vehicle speed is between 100 km/h and 120 km/h, the aerodynamic drag is 65% to 75% of the overall resistance (Zhu et al., 2012). Undoubtedly, the improvement of high-grade highways and the increase in vehicle speed have urged the meticulous aerodynamic design of vehicles for improving their fuel economy. The aerodynamic drag coefficient (Cd) is a critical metric that quantifies vehicle resistance in a fluid and is highly sensitive to the object's

*Corresponding author: Peng Hu, hupeng.kc@crrcgc.cc

shape and surface characteristics. Therefore, this study investigates the effect of windshield angle variation on the drag coefficient of an SUV using Computational Fluid Dynamics (CFD) analysis.

CFD is a technique for analyzing physical phenomena such as fluid flow and heat transfer through numerical simulation using a computer. CFD technology can analyze the phenomena in the flow field and display them using computers, allowing for a flow field prediction in a short time. This simulation tool can help understand fluid mechanics, guide experiments, and provide references for design, saving human resources, material resources, and time. CFD has already been extensively explored to address problems in vehicle aerodynamics. Numerous studies have demonstrated that reducing the aerodynamic drag experienced by a vehicle directly contributes to improved fuel economy and reduced emissions, outcomes that are of paramount importance in the context of increasingly stringent environmental regulations.

2. Literature review

The aerodynamic behavior of road vehicles has been extensively investigated using both experimental and computational approaches. Foundational studies on simplified bluff bodies, such as the Ahmed model, established the critical influence of rear slant angle on wake topology and drag coefficient (Ahmed et al., 1984). These investigations revealed that pressure drag, primarily generated at the rear of the vehicle, constitutes the dominant component of total aerodynamic resistance. Subsequent work by Lienhart and Becker (2003) provided comprehensive experimental datasets of flow and turbulence fields around the Ahmed body, which have since served as benchmarks for validating numerical turbulence models (Serre et al., 2013). These studies underscore the complexity of separated flows behind vehicle geometries and the challenges inherent in their accurate numerical prediction.

In the context of front-end geometry, the windshield angle has been identified as a parameter that significantly influences aerodynamic performance. Early work by Heald (1933) recognized the connection between streamlined shapes and reduced fuel consumption, while more recent parametric analyses have quantified the effect of windshield inclination on drag. For instance, Zhu et al. (2012) and Vignesh et al. (2019) performed CFD simulations on simplified sedan models, demonstrating that drag coefficient generally increases with steeper windshield angles. Bayindirli and Çelik (2020) reported a similar trend for a bus model, noting that drag could be reduced by up to 17.9% when the windshield inclination was optimized. Li et al. (2025) further included windshield angle as a key variable in a multi-parameter optimization of a passenger car, identifying an optimal value of 25° for their specific configuration. While these studies collectively establish the importance of windshield geometry, they are predominantly limited to passenger car or bus configurations. Moreover, the parametric ranges explored are often narrow, and the numerical methodologies—frequently relying on standard RANS models without rigorous mesh independence verification—vary considerably in their reported accuracy.

Parallel research efforts have focused on developing and validating CFD methodologies for realistic automotive geometries. The introduction of the DrivAer model provided a publicly available, industry-relevant benchmark that bridges the gap between simplified bluff bodies and proprietary production vehicle data (Elrefaie et al., 2025). Extensive numerical studies on the DrivAer model have compared the predictive capabilities of various RANS and hybrid RANS-LES approaches, generally concluding that eddy-resolving methods offer superior accuracy in capturing wake dynamics and force coefficients (Ashton et al., 2016). However, the computational cost of such methods remains prohibitive for large parametric sweeps, and well-validated steady RANS approaches continue to be widely employed in industrial practice (Almaghrebi & Ali, 2026; Bounds et al., 2020). These latter studies emphasize the critical importance of systematic mesh independence analysis and appropriate near-wall treatment to ensure reliable drag predictions. Furthermore, Elrefaie et al. (2025) quantified the contributions of specific vehicle components to overall drag, reporting that exterior mirrors add approximately 14–16 counts, while the inclusion of rotating wheels and a detailed underbody can increase drag by over 100 counts relative to simplified configurations.

Despite the breadth of existing literature, a notable gap persists. The aerodynamic influence of windshield angle on Sport Utility Vehicles (SUVs) remains comparatively underexplored. SUVs are characterized by bluff rear geometries and larger frontal areas, which result in distinct wake structures and a higher proportion of base pressure drag relative to sedans (Luckhurst et al., 2019; Wood et al., 2015). While studies such as that by Abdellah and Wang (2017) have examined windshield angle effects on a sedan, a dedicated, systematic parametric investigation isolating this variable on an SUV-class geometry has not been reported. Furthermore, many existing parametric CFD studies lack detailed documentation of mesh convergence criteria and near-wall resolution (y^+) validation, which are essential for establishing confidence in the quantitative trends observed (Almaghrebi & Ali, 2026; Wang & Hu, 2012).

Therefore, the novelty of the present work lies in providing a dedicated, high-resolution parametric quantification of the isolated effect of windshield angle on the aerodynamic drag of an SUV-class vehicle, using the 2013 BMW X5 as a representative geometry. This study distinguishes itself from prior work through three principal aspects: (i) the systematic variation of the windshield angle across a wide, practically relevant range of 30°–90°; (ii) the rigorous validation of the numerical setup, including a mesh independence study, near-wall y^+ verification, and explicit convergence criteria based on drag stabilization; and (iii) the provision of a clear, nearly linear quantitative relationship between windshield angle and Cd for an SUV, supported by detailed pressure and velocity field analyses. By addressing the methodological limitations noted in previous studies and focusing on a vehicle class of growing market significance, this work offers specific, actionable guidance for balancing aerodynamic efficiency with other design constraints in SUV development.

3. Geometry modelling

This work conducts CFD analysis on a BMW X5 (2013), which is an SUV selected based on the following criteria:

High car availability, as the BMW X5 is sold almost all over the world.

Officially provided specifications of the BMW X5 (2013) to facilitate the production of 3D models

The availability of the official drag coefficient (Cd) of the car allows checking the accuracy of the CFD results. The BMW X5 has a drag coefficient of 0.34 (Edmunds, 2013).

The car model is built using SolidWorks software, which will be saved in IGES format and imported into ANSYS software for CFD analysis. The model has been iterated several times to ensure its reliability, with the final car model and specifications illustrated in Figure 1. Parameters such as length, width, and height are provided by the official website (Figure 2, Table 1). In this study, the effect of windshield angle on the drag coefficient was evaluated by changing the front windshield angle.

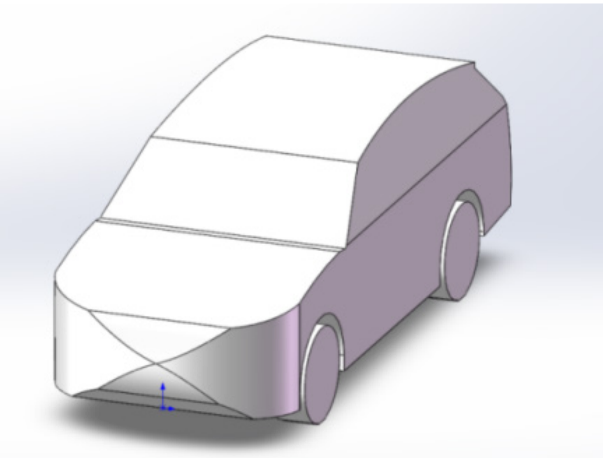

Figure 1: SolidWorks model of the BMW X5 (2013).

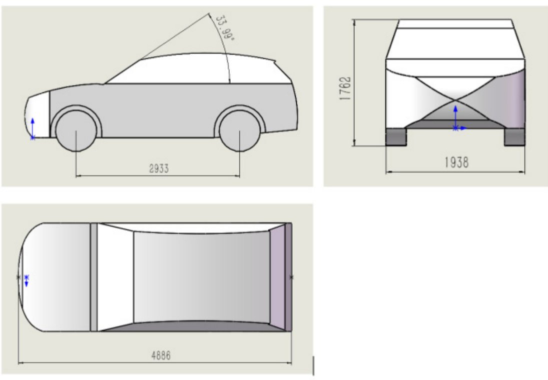

Figure 2: Orthogonal views of the car model.

Table 1: Specifications of the car model.

Specification	Data
Maximum height	1762 mm
Maximum width	1938 mm
Maximum length	4886 mm
Wheelbase	2933 mm
Windshield angle	33.99°

Several geometric simplifications were applied to the BMW X5 model for this parametric study. As shown in Figure 1, while the model retains the primary body contours and includes stationary wheels, it omits rearview mirrors, door handles, the antenna, and other minor protrusions. The underbody was also modelled as a smooth, continuous surface without detailed mechanical components.

These simplifications are deliberate and consistent with the objective of isolating the relative effect of windshield inclination on drag, rather than predicting the absolute Cd of a fully detailed production vehicle. Omitted components contribute to aerodynamic drag in a largely additive manner. Elrefaie et al. (2025) reported that exterior mirrors alone increase the drag coefficient of the DrivAer fastback model by approximately 15 counts, while the inclusion of rotating wheels and a detailed underbody adds over 100 counts. Simmonds et al. (2017) similarly noted that cooling drag and underbody complexity can alter the overall Cd by approximately 25 counts. In the present study, the numerically computed baseline Cd of 0.347 differs from the official value of 0.34 (Edmunds, 2013) by only 2.06%, a discrepancy consistent with the expected contributions of the omitted features.

Importantly, because the geometry of the omitted features remains unchanged across the entire parametric sweep of windshield angles, their aerodynamic contribution acts as a near-constant systematic offset. This offset does not materially influence the observed linear trend between windshield angle and drag coefficient. The strong correlation evident in Figure 10, together with the close agreement to the reference Cd, validates the suitability of this simplified modelling approach for the objectives of the present work.

4. Analysis in ANSYS fluent

Using CFD to analyze the vehicle's external flow field is divided into three steps: pre-processing, solving, and post-processing. Pre-processing transforms the specific problem into a computational domain and a grid acceptable to the solver. Although these two are only preparations for the solution process, they are time-consuming and play a decisive role in the accuracy of the solution results. After defining the boundary conditions, the pre-processing is completed. In this work, the pre-processing step uses ANSYS Workbench. Then, the pre-processing file is imported into the solver (Fluent 19) for calculation, and after setting various models and parameters, the iterative calculations start. Post-processing involves further refining the calculated results until intuitive and precise data and charts are obtained that are easy to communicate.

4.1. Creating an enclosure & Boolean

For the circulation around the vehicle, a fluid volume enclosure containing the car as the air domain was constructed, and the body was subtracted from the enclosure using a Boolean function. According to the vehicle dimensions, the final computational domain is a rectangular frame measuring 23 260 mm by 32 000 mm by 10 600 mm. The location of the enclosure and the vehicle is depicted in Figure 3, highlighting that the distance between the front of the car and the front of the enclosure is 5000 mm, which exceeds the length of the car body (4886 mm). The distance between the rear of the car and the end of the enclosure is 22 114 mm, which is more than 4.5 times the length of the car body. Additionally, 5.5 times the breadth of the car separates the left and right sides of the car from the enclosure (1938 mm). The enclosure is six times as tall as the car (1762 mm). A design modeler is also utilized to generate named selections, such as inlet, outlet, symmetric plane, wall-car, and wall-ground.

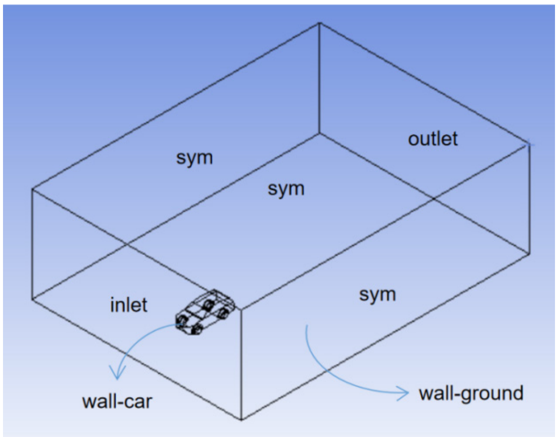

Figure 3: Enclosure.

4.2. Meshing

Mesh division is the discretization of the computing area, i.e., the spatially continuous computing area is divided into many sub-areas, and the nodes in each region are determined. In 3D models, FLUENT uses tetrahedra, hexahedra, pyramids, and wedge elements to form meshes, with this study using the tetrahedral mesh owing to its ease of generation and the high degree of approximation to the wall. However, the number of generated meshes is too large, imposing a significant calculation burden. The meshing algorithm uses Patch Conforming, and the Element Order is set to the Use Global Setting. In addition, Face Sizing is used to refine the mesh of the outer contour of the car. The Element Size and Growth Rate of the fine mesh are set to 25 mm and 1.1, respectively, allowing for accurate CFD simulation results. The CFD uses the Mesh Physics Preference, the Size function is Curvature, and the maximum surface size is set to 200 mm. The detailed mesh division settings are presented in Figure 4.

Details of "Mesh"

Defaults	
Physics Preference	CFD
Solver Preference	Fluent
Export Format	Standard
Export Preview Surface Mesh	No
Element Order	Linear
Sizing	
Size Function	Curvature
Max Face Size	200.0 mm
Mesh Defeaturing	Yes
Defeature Size	Default (1.0 mm)
Growth Rate	Default (1.20)
Min Size	10.0 mm
Max Tet Size	Default (400.0 mm)
Curvature Normal Angle	Default (18.0 °)

Details of "Face Sizing" - Sizing

Scope	
Scoping Method	Named Selection
Named Selection	wall-car
Definition	
Suppressed	No
Type	Element Size
Element Size	25.0 mm
Advanced	
Defeature Size	Default (1.0 mm)
Size Function	Uniform
Behavior	Soft
Growth Rate	1.1

Details of "Patch Conforming Method" - Method

Scope	
Scoping Method	Geometry Selection
Geometry	1 Body
Definition	
Suppressed	No
Method	Tetrahedrons
Algorithm	Patch Conforming
Element Order	Use Global Setting

Figure 4: Meshing settings.

4.2.1. Mesh independence verification

To ensure that the computed drag coefficient is not unduly sensitive to spatial discretization, a mesh independence study was conducted on the baseline configuration with a windshield angle of 30°. Three unstructured tetrahedral meshes of progressively increasing resolution were generated, designated as coarse, medium, and fine. The corresponding mesh parameters are summarised in Table 2. The medium mesh resolution corresponds to the settings subsequently employed for all parametric variations presented in Section 5.

In addition to the mesh resolution characterized by element count, the geometric quality of the computational cells constitutes a critical determinant of numerical accuracy and solution stability. A widely adopted metric for assessing mesh quality in unstructured tetrahedral grids is the cell skewness, which quantifies the deviation of a cell from its ideal equilateral shape. For the three mesh densities employed in the independence study, the arithmetic mean skewness values were 0.213 for the coarse mesh, 0.212 for the medium mesh, and 0.211 for the fine mesh, as summarised in Table 2. According to established quality guidelines for the ANSYS Fluent

Table 2: Summary of mesh parameters employed in the mesh independence study.

Mesh designation	Element size	Curvature min size	Face sizing on vehicle	Elements	skewness
Coarse	235mm	12mm	29mm	3804278	0.21328
Medium	200mm	10mm	25mm	5338269	0.21209
Fine	160mm	8mm	20mm	8793136	0.2112

solver, a mean skewness below 0.25 is indicative of a high-quality mesh suitable for reliable engineering computations, while a maximum skewness below 0.95 is generally considered acceptable for convergence. The maximum skewness values recorded across the three configurations were 0.935 for the fine mesh, 0.880 for the coarse mesh, and 0.855 for the medium mesh. Although the maximum skewness in the fine mesh marginally exceeds 0.9, inspection of the mesh topology confirmed that these highly skewed elements are confined to a small region near the far-field boundaries of the computational domain, remote from the vehicle surfaces. Consequently, they exert negligible influence on the near-body flow resolution and on the integral aerodynamic forces.

Each mesh was solved using the identical numerical settings detailed in Sections 4.3–4.8, with the simulation advanced to 3000 iterations. Given the inherent unsteadiness present in the near-wake region of bluff-body flows, strict residual convergence to machine precision is seldom attainable with steady-state RANS solvers (Almaghrebi & Ali, 2026). Consequently, the drag coefficient was monitored over the final 200 iterations, and the arithmetic mean value over this interval was adopted as the representative Cd for each mesh level. This practice of averaging over a statistically stationary segment of the iteration history aligns with established mesh independence analysis procedures for external automotive aerodynamics (Azman et al., 2025).

Table 3: Drag coefficient results obtained from the mesh independence study.

	Final Cd (3000 iterations)	Mean Cd (last 200 iterations)
Mesh (coarse)	0.3566	0.3579
Mesh (medium)	0.3503	0.3482
Mesh (fine)	0.3411	0.3411

Table 3 presents the drag coefficient results obtained from the mesh independence study. The relative difference in the mean Cd between the coarse and medium meshes was approximately 2.80%, while the difference between the medium and fine meshes reduced to 2.06%. According to the Grid Convergence Index (GCI) methodology proposed by Celik et al. (2008), this monotonic reduction in discretisation error indicates that the solution lies within the asymptotic range of convergence. Moreover, the sub-3% variation between the medium and fine meshes is considered acceptable for external automotive aerodynamics, where the complexity of separated flow structures introduces inherent variability that outweighs marginal gains from further mesh refinement (Almaghrebi & Ali, 2026; Azman et al., 2025).

Based on this analysis, the medium mesh configuration, comprising approximately 5.34 million cells, was deemed to offer a satisfactory compromise between numerical accuracy and computational expenditure. This mesh density was therefore adopted for all subsequent simulations in which the windshield angle was systematically varied from 30° to 90°.

4.3. Model setup

The analysis type for this study is a pressure-based steady-state solver, which is appropriate for the incompressible flow conditions considered here. The RNG k–ε turbulence model was selected for this investigation based on its demonstrated accuracy and robustness in simulating external automotive flows. Compared to the standard k–ε model, the RNG variant incorporates an analytically derived differential formulation for the effective viscosity and accounts for the effects of swirl and high strain rates—features that are particularly relevant to the flow over the A-pillar and windshield regions (Wang & Hu, 2012). Prior validation studies on simplified vehicle geometries have shown that the RNG k–ε model yields significantly better agreement with experimental drag coefficients than the standard k–ε formulation, with reported errors below 3% for bluff-body configurations (Wang & Hu, 2012). Furthermore, the RNG k–ε model offers a favorable balance between computational efficiency and predictive capability for flows involving moderate separation and streamline curvature, making it well suited for parametric investigations involving multiple geometric configurations (Kim, 2005). Although the k–ω SST model is known to provide improved near-wall resolution in flows with strong adverse pressure gradients, its higher sensitivity to inlet turbulence conditions and more stringent near-wall mesh requirements were considered less compatible with the present parametric study, which prioritized numerical stability and computational economy across thirteen distinct windshield angles. Accordingly, the RNG k–ε model was adopted for all simulations reported in this work.

4.4. Selection of wall functions

Standard Wall Functions, Enhanced Wall Treatment, and Non-Equilibrium Wall Functions are some of the wall function treatment methods available in FLUENT. The Standard Wall Functions method provides the necessary wall boundary conditions (for a balanced turbulent boundary layer) using a logarithmic correction. The Non-Equilibrium Wall Functions method is used to improve the results of high-pressure gradients, separation, reattachment, and stagnation. Both the Standard Wall Functions method and the Non-Equilibrium Wall Functions method use a relatively

Table 4: Comparison of near-wall treatments.

Function type	Advantage	Disadvantage
Standard Wall Functions	The treatment has a wide range of applications, requires minimal calculation, and achieves high precision.	The treatment is suitable for high Reynolds number flows. It is unsuitable for problems involving low Reynolds number flow, pressure gradients, high transpiration, large body forces, and high-velocity three-dimensional flow.
Non-Equilibrium Wall Functions	The treatment takes into account pressure gradients and can be applied to detachment, reattachment, and impact problems.	This treatment is not suitable for low Reynolds number flow problems, as it has strong pressure gradient problems, strong body force, and strong three-dimensionality problems.
Enhanced Wall Treatment	The treatment does not depend on the wall law and is suitable for complex flows, especially low Reynolds number flows.	The dense mesh is required, so the computer needs an extended processing time and a large memory.

coarse mesh in the near-wall region. Standard or Non-Equilibrium Wall Functions (Re>10°) can be used for most high Reynolds number cases. Finally, the Enhanced Wall Treatment option combines the mixed boundary model with the two-layer boundary model, which is suitable for low Reynolds number flows or complex near-wall phenomena because the turbulence model has been corrected on the inner layer. Table 4 summarizes the advantages and disadvantages of the three wall functions. After careful consideration, this study adopts the Standard Wall Functions for its CFD analysis.

The appropriateness of the near-wall mesh resolution for the Standard Wall Functions employed in this study was evaluated by examining the distribution of the dimensionless wall distance y^+ along the vehicle surface. Figure 5 presents the y^+ values extracted along the longitudinal centreline of the baseline model (30° windshield) using the medium mesh configuration after 800 iterations. The majority of the sampled points exhibit y^+ values in the range of 30 to 140, which falls well within the recommended bounds for Standard Wall Functions in external automotive aerodynamics (Almaghrebi & Ali, 2026; Salim & Cheah, 2009). Localised excursions to values slightly below 30 are observed near the front stagnation region and at the base of the windshield. Such departures are attributable to locally reduced wall shear stress in stagnation and separation zones, a behaviour commonly encountered in bluff-body flows (Almaghrebi & Ali, 2026). As noted by Salim and Cheah (2009), limited excursions of this

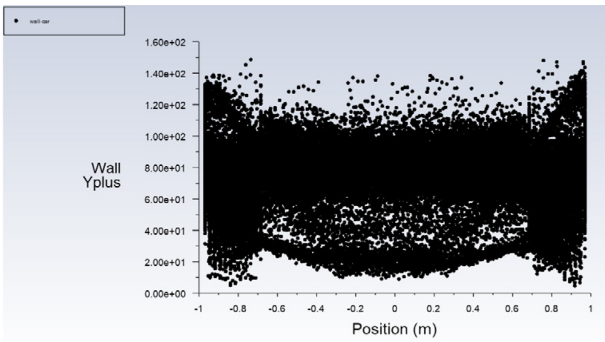

Figure 5: Wall y+ distribution along the vehicle centreline (medium mesh, 30° windshield, 800 iterations).

nature do not compromise the overall validity of the wall-modelled approach, provided that the bulk of the boundary layer resides within the logarithmic region. Consequently, the present mesh is deemed to furnish an appropriate near-wall resolution for the RANS simulations reported in this study.

4.5. Boundary conditions

Boundary and initial conditions are the prerequisites for the definite solution of the governing equations. The boundary condition is the rule that the variables or their derivatives to be solved change with time and place on the boundary of the solution area. Any problem requires boundary conditions. The initial condition is the spatial distribution of each solution variable of the object being analyzed by the user. The processing of initial and boundary conditions will have a direct effect on the precision of the calculated results.

In this study, the enclosure inlet is defined as the velocity inlet. Assuming that the velocity is perpendicular to the boundary surface and the absolute value of the velocity is 10 m/s, the temperature is defined as 300 K. The enclosure outlet and the symmetry plane are defined as the pressure outlet. The Initial Gauge Pressure of both the pressure outlet and the velocity inlet is 0 Pascal. The wall-car and wall-ground are stationary walls with "no slip" shear conditions.

The uniform inlet velocity was prescribed as 10 m/s. While lower than typical highway speeds, this choice is well-justified for the present parametric study. The primary objective is to resolve the relative influence of windshield angle on the drag coefficient (Cd), rather than predicting absolute values at a specific high speed. In incompressible external aerodynamics, Cd is governed by the Reynolds number (Re). For bluff bodies at sufficiently high Re, the flow enters a fully turbulent regime where aerodynamic coefficients become largely insensitive to further increases in Re, a condition known as Reynolds number independence (Almaghrebi & Ali, 2026). The Re based on model length for the 10 m/s case is approximately 3.3×10^6, placing it well within this regime.

A supplementary simulation on the medium grid at a 30° windshield angle using an inlet velocity of 25 m/s further supports this approach. Table 5 compares the computed Cd at the 800th iteration for both velocities. The values—0.3461 at 10 m/s and 0.3337 at 25 m/s—exhibit a variation consistent with the modest Reynolds number effect expected in this range. Critically, the flow topology governing the drag trend remains consistent between the two cases, confirming that 10 m/s is adequate for capturing the parametric sensitivity.

Table 5: Comparison of computed drag coefficient (Cd) at two inlet velocities after 800 iterations.

Inlet speed	Final Cd (800 iterations)
10 m/s	0.3461
25 m/s	0.3337

Beyond scientific validity, the 10 m/s velocity offers tangible computational benefits for a multi-case parametric investigation. It reduces Courant-Friedrichs-Lewy (CFL) number constraints, thereby improving solver stability and accelerating convergence (Ramnefors et al., 1996). Employing a moderate Reynolds number to study fundamental aerodynamic trends is an established and cost-effective practice in automotive CFD (Bounds et al., 2020).

4.6. Reference values

It is essential to set the correct Reference Values when calculating drag or moment coefficients. The primary focus of this study is calculating the drag coefficient, which involves adjusting two reference values according to the calculation formula: speed and area. The reference value of velocity is 10 m/s, which is equal to the velocity of the entrance. The reference value of the area is 3.05 m^2, which is calculated based on the frontal area of the model. Besides, the reference values of density and viscosity are 1.225 kg/m^3 and 1.7894×10^{-05} kg/m·s, respectively, which are properties of air. To better evaluate the impact of windshield angle changes on vehicle drag coefficient, CFD analysis for models with different windshield angles will adopt the same reference values presented above.

4.7. Initialization settings

Before starting the calculations, an initial value must be set for the flow field, with the related process of setting the initial value called "initialization". Suppose the flow field solutions obtained by each step of iteration are arranged in a sequence. In that case, the initial value is the first number in the sequence, and the solution that reaches the convergence condition is the last number. Obviously, if the initial value is closer to the final convergent solution, the calculation speed will be accelerated. Otherwise, increasing the number of iteration steps will lengthen the calculation process. Notably, if the initial value is not set correctly, the convergent solution may not be obtained. This study uses Standard Initialization, and the specific setting parameters are presented in Figure 6.

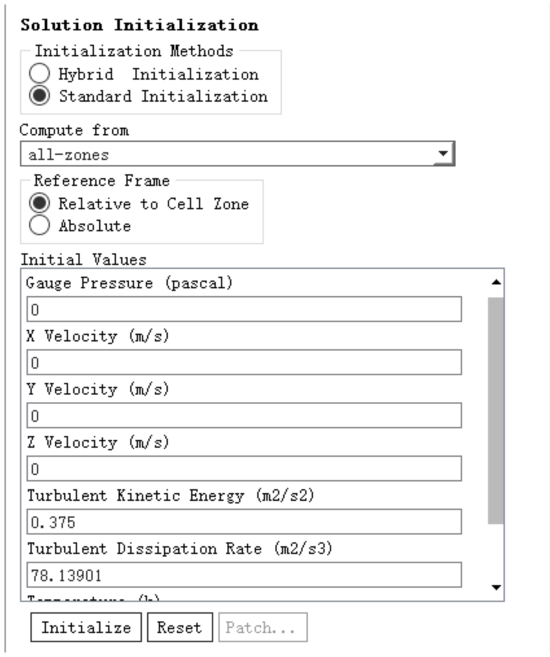

Figure 6: Initialization settings.

4.8. Solution Methods Settings

The pressure-based solver was employed in this study, consistent with the incompressible flow assumption. To identify the most robust pressure–velocity coupling scheme for the current configuration, a systematic comparison of the SIMPLE, SIMPLEC, PISO, and Coupled algorithms was conducted. The primary criterion for selection was the convergence behaviour of the drag coefficient (Cd) and the associated residuals, given the practical constraint of limiting each simulation to 800 iterations to manage the computational cost of the parametric sweep.

All four schemes were evaluated on the identical medium-density mesh using the same boundary conditions. The Cd values predicted at the final iteration were 0.34703459 (SIMPLE), 0.34706998 (SIMPLEC), 0.34678508 (PISO), and 0.33727939 (Coupled). While the segregated algorithms (SIMPLE, SIMPLEC, and PISO) yielded closely comparable drag predictions, the Coupled scheme produced a notable deviation. More importantly, the residual histories presented in Figure 7 reveal significant differences in numerical stability. The Coupled algorithm exhibited persistent and severe oscillations, indicating poor convergence characteristics. In contrast, the SIMPLEC scheme demonstrated the most rapid and monotonic reduction in residuals.

Based on its superior convergence behaviour and a Cd prediction consistent with the other segregated schemes, the SIMPLEC algorithm was selected for all subsequent simulations. For all computations, spatial discretization was achieved using second-order upwind schemes for momentum, turbulent kinetic energy, and turbulent dissipation rate. Pressure and gradient terms were treated with second-order and least-squares cell-based formulations, respectively.

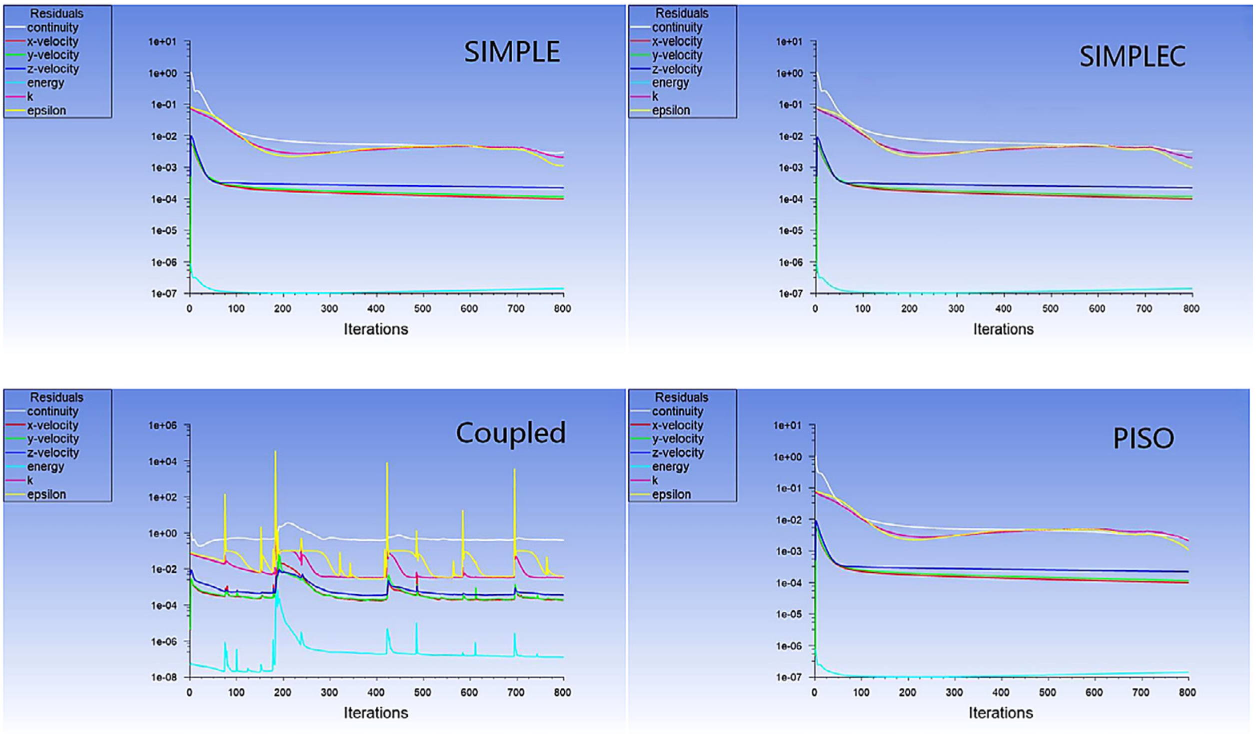

Figure 7: Convergence history of residuals for the evaluated pressure–velocity coupling algorithms over 800 iterations.

4.9. Convergence assessment

In this study, the stabilisation of the drag coefficient (Cd) was adopted as the primary convergence criterion. For steady-state RANS simulations of bluff-body flows, achieving strict residual convergence to machine precision is seldom practical due to the inherent unsteadiness present in the near-wake region. As an alternative, the stabilisation of integral force quantities, particularly the drag coefficient, is widely adopted as a reliable indicator of engineering convergence (Makowski & Kim, 2000).

Figure 8 presents the Cd history over 3000 iterations for the baseline 30° windshield configuration obtained using the medium mesh. The drag coefficient exhibits a rapid initial transient phase within the first 400 iterations, followed by a statistically stationary oscillatory pattern. The Cd value at 800 iterations (0.3461) differs by less than 1.2% from that at 3000 iterations (0.3503), and by less than 0.6% from the mean value of the final 200 iterations (0.3482). According to established practice in applied aerodynamics, such a small variation in the monitored force quantity indicates that the solution has reached a sufficiently converged state for engineering purposes (Roger et al., 2011). Consequently, 800 iterations were deemed adequate for the parametric sweep simulations, while a more extended iteration count was employed for the mesh independence verification to provide a conservative benchmark.

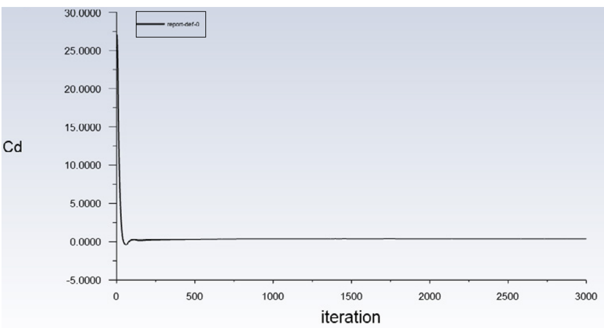

Figure 8: Evolution of the drag coefficient over 3000 iterations for the baseline 30° windshield configuration using the medium mesh.

4.10. Adjustment of model windshield

This study primarily investigates the impact of windshield angle on the car's drag coefficient as the windshield angle changes from 30°- 90°, while the other model parameters remain unchanged. Figure 9 depicts the car model under various windshield angles.

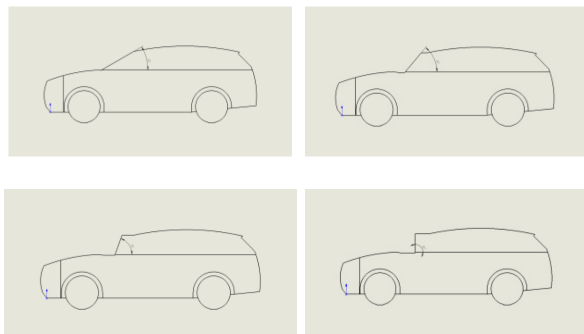

Figure 9: Car models with windshield angles of 30°, 50°, 70°, and 90°.

Windshield angle	Drag coefficient
30	0.34608441
33.99	0.34706998
35	0.35078156
40	0.35492314
45	0.36118304
50	0.36473885
55	0.37303108
60	0.37890311
65	0.39061121
70	0.39631725
75	0.40255918
80	0.40877093
85	0.41040353
90	0.41508144

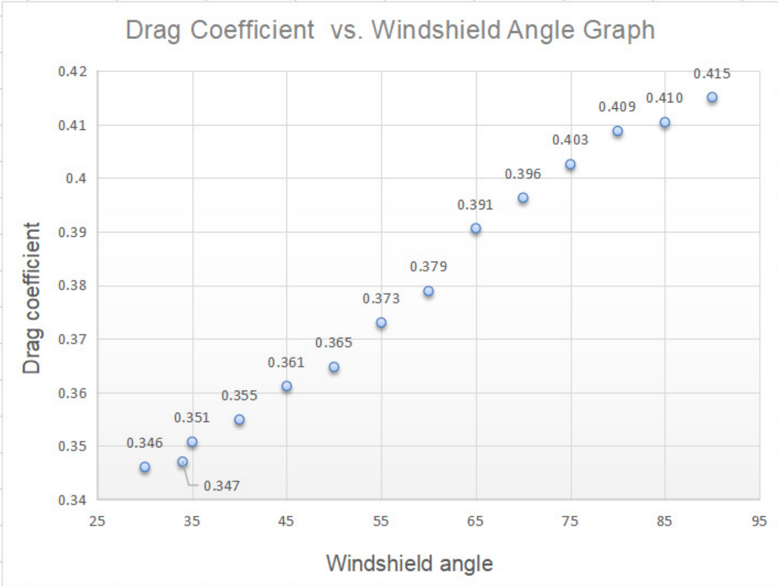

Figure 10: Effect of windshield angle on drag coefficient.

5. Results and discussion

5.1. Drag coefficient trend

The numerically predicted drag coefficients (Cd) for windshield angles ranging from 30° to 90° are presented in Figure 10. A clear, nearly linear relationship is observed: Cd increases monotonically from a minimum of 0.346 at 30° to a maximum of 0.415 at 90°. This trend is consistent with the increased obstruction presented by a steeper windshield, which amplifies the pressure drag component that dominates the overall aerodynamic resistance of bluff bodies (Zhu et al., 2012). To elucidate the underlying flow physics responsible for this increase, the following sections examine the corresponding pressure and velocity fields in detail.

5.2. Pressure distribution and its contribution to drag

Aerodynamic drag is primarily composed of pressure drag and friction drag, with the former accounting for approximately 90% of the total resistance for typical road vehicles (Zhu et al., 2012). Figure 11 displays the static pressure contours on the vehicle surface across the range of windshield angles. Two distinct effects are evident as the windshield angle increases. First, the local surface pressure on the windshield itself rises substantially, from approximately 14.2 Pa at the base for the 30° configuration to 26.3 Pa for the 90° configuration. Second, the spatial extent of the high-pressure region on the windshield expands, progressively encroaching toward the roof at steeper angles. This is further corroborated by the front pressure distribution contours shown in Figure 13, where the high-pressure zones on the windshield become both larger and more intense as the angle steepens.

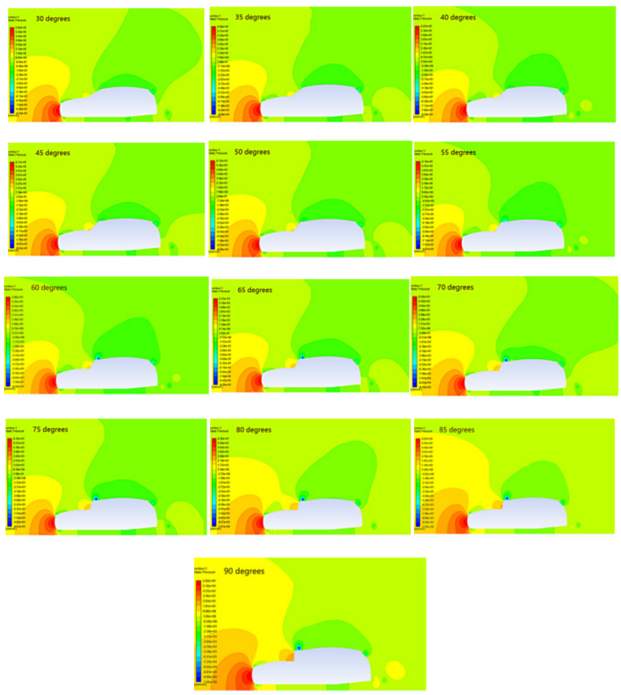

Figure 11: Pressure contour.

These observations are directly linked to the velocity vector fields depicted in Figure 12. At a shallow 30° angle, the velocity vectors indicate that the flow is deflected upward with minimal stagnation; the low-velocity region at the windshield base is relatively small, and the airflow maintains a high speed as it travels over the roof. As the angle increases to 50° and 70°, the windshield acts as an increasingly bluff obstruction. The flow decelerates more abruptly upon impact, leading to a larger stagnation zone and the formation of a prominent recirculation vortex near the top of the windshield. At 70°, the velocity vectors also reveal a substantial portion of the flow being diverted laterally around the A-pillars rather than traveling over the roof. At 90°, the windshield becomes a near-normal

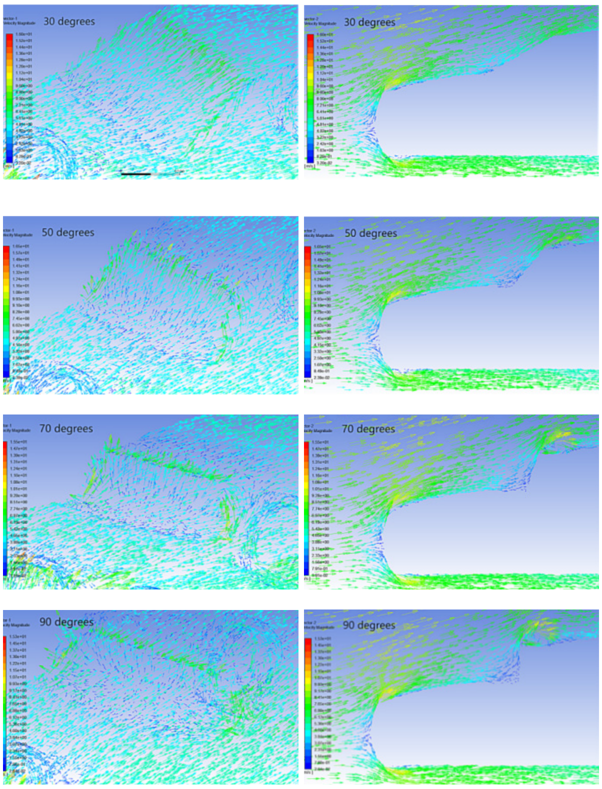

Figure 12: Velocity vector diagrams of the model for 30°, 50°, 70°, and 90° for windshield angle.

barrier to the flow, resulting in the most extensive low-velocity region and the highest surface pressures. The speed of the flow impinging on the windshield drops to as low as 0.0264 m/s in this extreme case. This amplified adverse pressure gradient on the forward-facing surface directly increases the pressure drag.

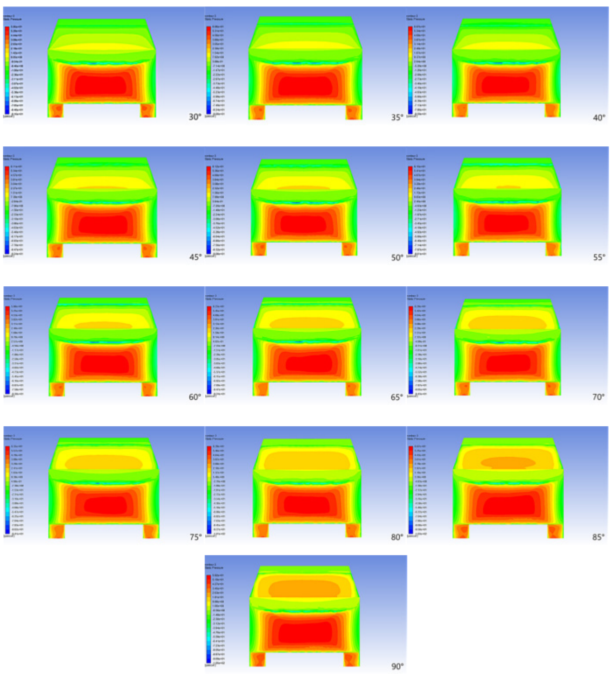

Figure 13: Front pressure distribution contour.

In contrast, the pressure distribution on the front fascia and the rear surfaces of the vehicle remains largely unchanged across the parametric sweep, as shown in Figures 13 and 14. The front stagnation pressure exhibits only modest fluctuations (ranging from 59.2 Pa to 63.5 Pa) without a clear monotonic trend, confirming that the observed drag increase is predominantly driven by the modified flow physics on the windshield itself, rather than by substantial changes to the forebody stagnation or the wake structure.

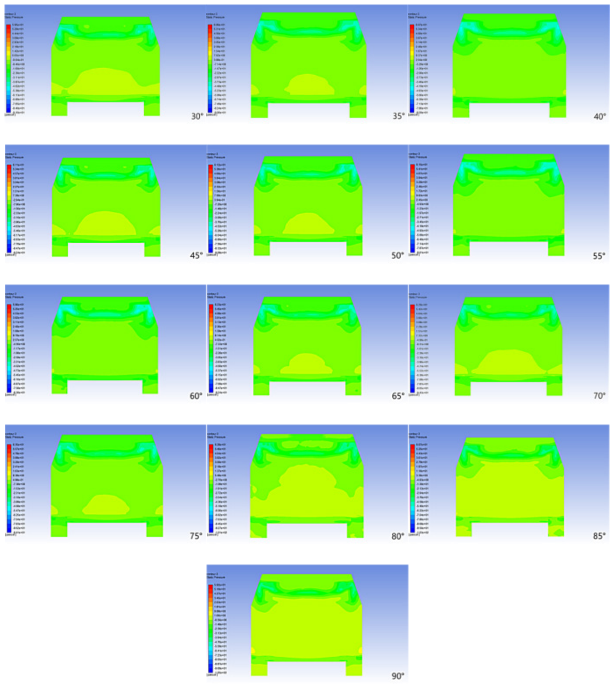

Figure 14: Back pressure distribution contour.

5.3. Velocity field and wake characteristics

The velocity contour plots in Figure 15 further illustrate the flow deceleration at the windshield. A low-velocity zone at the base of the windshield expands markedly as the inclination angle increases, consistent with the intensified stagnation observed in the vector fields. This behavior confirms that steeper windshields promote more severe flow separation and energy dissipation in the forward region of the vehicle.

With regard to the vehicle wake, the velocity contours in Fig. 15 and the rear pressure distributions in Figure 14 indicate that the macroscopic structure of the wake does not vary substantially with windshield angle. This is a physically plausible outcome, as the wake topology of an SUV is primarily dictated by the rear-end geometry—specifically the rear glass angle, the base contour, and the underbody configuration—all of which were held constant in this study. While the windshield angle alters the trajectory and energy of the flow over the roof, its influence on the final detachment point and the large-scale recirculation behind the vehicle appears to be secondary. Consequently, the aerodynamic penalty associated with steeper windshield angles stems

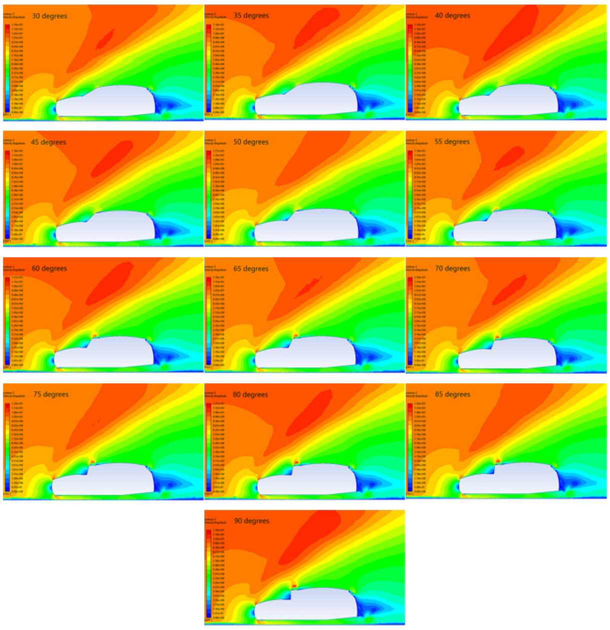

Figure 15: Velocity contour.

principally from increased pressure drag on the forward-facing surfaces, rather than from significant modifications to base pressure or wake dynamics.

5.4. Assessment of Velocity Field Development

It is pertinent to comment on the velocity contour data presented in Figure 15, which were obtained after 800 iterations. As discussed in Section 14, the integral quantity of primary interest—the drag coefficient—was demonstrably stabilized at this iteration count. However, the detailed velocity field in the near-body region, particularly over the roof, had not yet attained its fully developed spatial distribution. To provide a more physically representative qualitative visualization, an additional simulation was performed for the baseline 33.99° configuration and advanced to 2000 iterations. The resulting velocity contour, shown in Figure 16, exhibits the expected flow topology, with the maximum streamwise velocity correctly situated over the vehicle roof. This supplementary simulation confirms the physical soundness of the numerical setup and provides a more instructive qualitative reference for the flow field, while the quantitative trends reported for Cd are robustly supported by the 800-iteration parametric sweep.

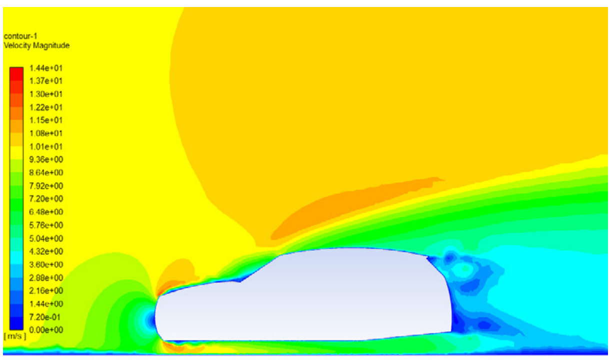

Figure 16: The newly obtained velocity contour diagram with 2000 iteration steps.

6. Conclusion

This study established a rigorous computational framework to investigate the influence of windshield angle on the aerodynamic performance of SUVs, using a simplified 3D model of the 2013 BMW X5. Through systematic CFD analysis via ANSYS Fluent, the relationship between windshield inclination and drag coefficient (Cd) was quantified across a practical range of 30–90°. The numerical methodology was extensively validated through a mesh independence study, near-wall y^+ verification, and explicit convergence criteria based on drag stabilization, thereby ensuring the robustness of the parametric trends observed and addressing common methodological limitations in the literature.

The key findings revealed a nearly linear correlation between windshield angle and aerodynamic drag, with Cd increasing from 0.346 at 30° to 0.415 at 90°. Pressure contour analysis demonstrated that this trend is primarily driven by increased surface pressure on the windshield itself, which rises from approximately 14.2 Pa to 26.3 Pa as the angle steepens. Velocity vector and contour analyses further elucidated the underlying flow physics: steeper windshields act as increasingly bluff obstructions, promoting more abrupt flow deceleration, enlarging the stagnation zone at the windshield base, and generating stronger recirculation vortices. In contrast, the front fascia and rear base pressure distributions remained largely unchanged, confirming that the observed drag increase is predominantly attributable to the increased pressure drag on the forward-facing surfaces, rather than to substantial modifications in the base wake structure.

The baseline configuration (33.99°) yielded a numerically predicted Cd of 0.347, differing from the official value of 0.34 by only 2.06%. This close agreement, together with the consistent linear trend observed across the parametric sweep, validates the reliability of the computational approach and the suitability of the simplified modelling strategy for the objectives of this work.

This research contributes to automotive aerodynamic design by providing quantifiable, actionable guidance for windshield angle optimization. The observed linear relationship enables designers to predict drag coefficient changes associated with windshield inclination adjustments, thereby facilitating informed trade-offs between aerodynamic efficiency and competing design constraints such as driver visibility and passenger headroom.

Future work will extend this investigation by incorporating additional geometric details—including rearview mirrors, windshield curvature, and underbody complexity—to better approximate real-world conditions. Furthermore, the combined effects of multiple geometric parameters, such as rear glass angle and hood inclination, will be explored using orthogonal test methods to develop a more comprehensive aerodynamic optimization strategy for SUV bodies.

Acknowledgements

Boyuan DU would like to express sincere gratitude to Peng Hu, Director of CRRC Technology Innovation No.10 Research Institute, for his valuable guidance on research design and manuscript revision. Special thanks are extended to CRRC Technology Innovation (Beijing) Co., Ltd for providing the necessary research conditions. The authors also appreciate the constructive feedback from colleagues and reviewers that improved the quality of this manuscript.

Funding

For single agency grants: 'This work was supported by the CRRC Technology Innovation (Beijing) Co., Ltd.

Author Contributions

Boyuan DU: Conceptualization (lead); Methodology (lead); Formal analysis (lead); Writing – original draft (lead); Writing – review and editing (equal); Peng Hu: Conceptualization (supporting); Validation (supporting); Project administration (supporting); Writing – review and editing (equal); Wenyao Zou: Software (lead); Investigation (supporting); Writing – review and editing (supporting); Xiangyu Xin: Investigation (supporting); Writing – review and editing (supporting).

Conflicts of Interest

The authors declare no conflicts of interest.

Declaration of generative AI and AI-assisted technologies in the writing process

During the preparation of this work the author(s) used ChatGPT in order to assist with language refinement and editorial suggestions. After using this tool/service, the author(s) reviewed and edited the content as needed and take(s) full responsibility for the content of the publication.

References

Abdellah, E., & Wang, B. (2017, 28-30 July). CFD analysis on effect of front windshield angle on aerodynamic drag. In, *2017 2nd International Seminar on Advances in Materials Science and Engineering* (pp. 012173), Singapore: IOP Publishing. https://doi.org/10.1088/1757-899X/231/1/012173

Ahmed, S. R., Ramm, G., & Faltin, G. (1984, 27 February). *Some salient features of the time-averaged ground vehicle wake. In, SAE International Congress and Exposition* (pp. 840300), Detroit, Michigan, United States: SAE International. https://doi.org/10.4271/840300

Almaghrebi, M., & Ali, A. A. E. (2026). Mesh independence and reynolds number sensitivity for external automotive aerodynamics simulations. *Scientific Journal of Engineering Research, 2*(1), 1-14. https://doi.org/10.64539/sjer.v2i1.2026.353

Ashton, N., West, A., Lardeau, S., & Revell, A. (2016). Assessment of RANS and DES methods for realistic automotive models. *Computers & Fluids, 128*, 1-15. https://doi.org/10.1016/j.compfluid.2016.01.008

Azman, A. N. N., Venkatason, K., & Sivaguru, S. (2025). Mesh convergence analysis on the aerodynamic performance of a sedan vehicle. *Journal of Engineering Technology and Applied Physics, 7*(1), 85-95. https://doi.org/10.33093/jetap.2025.7.1.14

Bayındırlı, C., & Çelik, M. (2020). The determination of effect of windshield ınclination angle on drag coefficient of a bus model by CFD method. *International Journal of Automotive Engineering and Technologies, 9*(3), 122-129. https://doi.org/10.18245/ijaet.723755

Bounds, C. P., Zhang, C., & Uddin, M. (2020). Improved CFD prediction of flows past simplified and real-life automotive bodies using modified turbulence model closure coefficients. *Proceedings of the Institution of Mechanical Engineers, Part D: Journal of Automobile Engineering, 234*(10-11), 2522-2545. https://doi.org/10.1177/0954407020916671

Celik, I. B., Ghia, U., Roache, P. J., & Freitas, C. J. (2008). Procedure for estimation and reporting of uncertainty due to discretization in CFD applications. *Journal of Fluids Engineering-Transactions of the ASME, 130*(7), 078001. https://doi.org/10.1115/1.2960953

Edmunds. (2013). Used 2013 BMW X5 SUV - Specs & Features. https://www.edmunds.com/bmw/x5/2013/suv/features-specs/?style=200420453

Elrefaie, M., Dai, A., & Ahmed, F. (2025). Drivaernet: A parametric car dataset for data-driven aerodynamic design and prediction. *Journal of Mechanical Design, 147*(4), 041712. https://doi.org/10.1115/1.4068104

Heald, R. H. (1933). Aerodynamic characteristics of automobile models. US Government Printing Office. https://doi.org/10.6028/jres.011.021

Kim, M. H. (2005). Aerodynamic simulation on the drag reduction device of a large-sized bus model. *International Journal of Heavy Vehicle Systems, 12*(3), 207-224. https://doi.org/10.1504/ijhvs.2005.008026

Li, J., Zhu, X., Zhang, C., Dang, S., & Chen, G. (2025). CFD simulation of passenger car aerodynamics and body parameter optimization. *Fluid Dynamics & Materials Processing, 21*(9), 2305. https://doi.org/10.32604/fdmp.2025.067087

Lienhart, H., & Becker, S. (2003). Flow and turbulence structure in the wake of a simplified car model. *SAE Transactions, 112*(6), 785-796. https://doi.org/10.4271/2003-01-0656

Luckhurst, S., Varney, M., Xia, H., Passmore, M. A., & Gaylard, A. (2019). Computational investigation into the sensitivity of a simplified vehicle wake to small base geometry changes. *Journal of Wind Engineering and Industrial Aerodynamics, 185*, 1-15. https://doi.org/10.1016/j.jweia.2018.12.010

Makowski, F. T., & Kim, S. E. (2000, 6 March). Advances in external-aero simulation of ground vehicles using the steady RANS equations. In, *SAE 2000 World Congress* (pp. 2000-2001-0484), Detroit, Michigan, United States: SAE International. https://doi.org/10.4271/2000-01-0484

Ramnefors, M., Bensryd, R., Holmberg, E., & Perzon, S. (1996, 26 February). Accuracy of drag predictions on cars using CFD-effect of grid refinement and turbulence models. In, *International Congress & Exposition* (pp. 960681), Detroit, Michigan, United States: SAE International. https://doi.org/10.4271/960681

Roger, R., Chan, S., & Smith, J. (2011, 27-30 June). Aerodynamic effects of external camera pods and launch lugs on a target missile configuration. In, *29th AIAA Applied Aerodynamics Conference* (pp. 3664), Honolulu, Hawaii: AIAA. https://doi.org/10.2514/6.2011-3664

Salim, S. M., & Cheah, S. (2009, 18-20 March). Wall Y strategy for dealing with wall-bounded turbulent flows. In, *Proceedings of the International Multiconference of Engineers and Computer Scientists* (pp. 2165-2170), Hong Kong, China: Springer Singapore. https://www.iaeng.org/publication/IMECS2009/IMECS2009_pp2165-2170.pdf

Serre, E., Minguez, M., Pasquetti, R., Guilmineau, E., Deng, G. B., Kornhaas, M., Schäfer, M., Fröhlich, J., Hinterberger, C., & Rodi, W. (2013). On simulating the turbulent flow around the Ahmed body: A French–German collaborative evaluation of LES and DES. *Computers & Fluids, 78*, 10-23. https://doi.org/10.1016/j.compfluid.2011.05.017

Simmonds, N., Pitman, J., Tsoutsanis, P., Jenkins, K., Gaylard, A., & Jansen, W. (2017, 4-6 April). Complete body aerodynamic study of three vehicles. In, *WCX™ 17: SAE World Congress Experience* (pp. TBMG-26520), Detroit, MI: SAE International. https://doi.org/10.4271/2017-01-1529

Vignesh, S., Gangad, V. S., V, J., Maheswarreddy, Krishna, A., & Mukkamala, Y. S. (2019). Windscreen angle and Hood inclination optimization for drag reduction in cars. *Procedia Manufacturing, 30*, 685-692. https://doi.org/10.1016/j.promfg.2019.02.062

Wang, J. Y., & Hu, X. J. (2012). Application of RNG k-ε turbulence model on numerical simulation in vehicle external flow field. *Applied Mechanics and Materials, 170*, 3324-3328. https://doi.org/10.4028/www.scientific.net/AMM.170-173.3324

Wood, A., Passmore, M., Forbes, D., Wood, D., & Gaylard, A. (2015). Base pressure and flow-field measurements on a generic SUV model. *SAE International Journal of Passenger Cars-Mechanical Systems, 8*(2015-01-1546), 233-241. https://doi.org/10.4271/2015-01-1546

Zhu, H., Yu, H., & Yang, Z. (2012, 7-9 December). Numerical analysis on effect of back/front windshied and hood angle on automotive aerodynamic drag [windshied read windshield]. In, *IET International Conference on Information Science and Control Engineering 2012* (ICISCE 2012) (pp. 1-25), Shenzhen, China: IET. https://doi.org/10.1049/cp.2012.2282